Linear and second-order optical response of III-V monolayer superlattices

S. Sharma,* J. K. Dewhurst, and C. Ambrosch-Draxl
Institute for Theoretical Physics, Karl-Franzens-Universität Graz, Universitätsplatz 5, A-8010 Graz, Austria
(Received 22 November 2002; published 30 April 2003)

We report the fully self-consistent calculations of the nonlinear optical properties of superlattices. The materials investigated are monolayer superlattices with GaP grown on the the top of InP, AlP, and GaAs (110) substrates. We use the full-potential linearized augmented plane-wave method within the generalized gradient approximation to obtain the frequency-dependent dielectric tensor and the second-harmonic-generation susceptibility. The effect of lattice relaxations on the linear optical properties is studied. Our calculations show that the major anisotropy in the optical properties is the result of strain in GaP. This anisotropy is maximum for the superlattice with the maximum lattice mismatch between the constituent materials. In order to differentiate the superlattice features from the bulklike transitions, an improvement over the existing effective-medium model is proposed. The superlattice features are found to be more pronounced for the second order than the linear optical response, indicating the need for full supercell calculations in determining the correct second-order response.

DOI: 10.1103/PhysRevB.67.165332 PACS number(s): 78.20.−e, 42.70.Mp

I. INTRODUCTION

Semiconducting strained superlattices (SL's) are potential materials for applications in optical communications involving switching, amplification, and signal processing. In particular, III-V semiconductor heterostructures and SL's have attracted a great deal of interest mainly due to the possibility of tailoring band gaps and band structures[1–5] by the variation of simple parameters such as superlattice period, growth direction, and substrate material. With the development of new techniques such as the strain induced lateral ordering process[6] and existing methods such as molecular beam epitaxy[7] and low-pressure chemical-vapor deposition,[8] it is possible to grow and tailor these SL's. Thus a great deal of experimental work has been devoted to these materials. The unusual optical behavior of AlP/GaP SL's has been extensively studied using photoluminescence, magnetophotoluminescence,[9–11] optical absorption,[12] x-ray diffraction,[13] and refractive index measurements.[14] InP/GaP, being one of the material combinations which spontaneously constructs the SL under specific conditions, has been subject to numerous experimental works[15–17] including cathodoluminescence experiments[18–20] and studies on the influence of pressure, SL period, and barrier thickness[21–23] on the optical transitions. Likewise, GaAs/GaP[24,25] and GaAs/AlAs[26–32] have also been extensively investigated in the past.

Much of the theoretical work done to explain these interesting physical properties of SL's has been largely concerned with the understanding of the electronic band structure. For example, the effect of strain on the band gap, the band offset problem and the possibilities of engineering it, as well as the interface energy and band structure have been studied.[33–42] The linear optical properties of SL's have also been determined theoretically. Franceschetti and Zunger have calculated the pressure coefficients of optical transitions in InP/GaP SL's.[43] The pseudopotential method within the local-density approximation (LDA) has been used by Kobayashi *et al.*[44] to calculate the optical transition strengths of $(AlP)_n/(GaP)_m$-type multi-quantum-well SL's and for GaAs/AlAs by Yee *et al.*[45] Confinement effects on optical transitions for various superlattice periods in GaAs/AlAs has been discussed by Schmid *et al.*[46] The sp^3s^* tight-binding method has been used for the study of optical properties and the indirect-to-direct band-gap transition of AlP/GaP (Refs. 47 and 48) and GaAs/AlAs SL's.[49] Botti and Andreani[50] have employed the linear combination of bulk bands method to determine the optical properties of GaAs/AlAs SL's and electroabsorption properties of these SL's have been studied by Kawashima and Fujiwara.[51] Shibata *et al.*[52] used the pseudopotential method to determine the oscillator strength and band structures of the AlP/GaP SL's.

Due to the breaking of the inversion symmetry at surfaces and interfaces, the nonlinear optical properties are more sensitive than the linear optical properties and so the second-harmonic generation (SHG) by some of these SL's has also been calculated and determined experimentally.[20] The major theoretical work in this direction was done by Ghahramani and Sipe.[53–56] They used the effective-medium model (EMM) to determine the linear and nonlinear optical properties of $(GaAs)_n/(GaP)_n$, $(Si)_n/(Ge)_n$, and $(GaAs)_n/(AlAs)_m$ SL's. They also employed the non-self-consistent linear-combination-of-Gaussian-orbitals (LCGO) method within the LDA to calculate the band structures and optical properties of these compounds. In these works, Ghahramani *et al.* conclude that away from the absorption edge, most of the features in the linear as well as nonlinear optical properties are due to the bulk transitions that are well modeled by the EMM.

There have been very few studies of the linear optical properties of SL's and even fewer calculations of the nonlinear properties. Also, the existing theoretical work is neither self-consistent nor takes into account the effect of lattice relaxations on the SL optical properties. Hence, there is a need for a fully self-consistent calculation of the nonlinear and linear optical properties of superlattices in conjunction with a study of the lattice relaxation effects. The aim of the present work is to calculate the linear and the nonlinear optical properties of III-V monolayer SL's using the state-of-the-art full-

TABLE I. Superlattice lattice parameters are in angstrom units. $a_{\parallel}=a_x=a_y$ and $a_{\perp}=a_z$ which is the direction of crystal growth.

Superlattice	$a_{\parallel}$	$a_{\perp}$
$(InP)_1/(GaP)_1$	4.150	5.660
$(AlP)_1/(GaP)_1$	3.933	5.457
$(GaAs)_1/(GaP)_1$	3.998	5.553

potential linearized augmented plane-wave method (FPLAPW). The materials investigated are $(InP)_1/(GaP)_1$, $(AlP)_1/(GaP)_1$, and $(GaAs)_1/(GaP)_1$. The EMM is also tested for all these materials. For InP/GaP and AlP/GaP, this model fails to reproduce even the features away from the absorption edge. So the EMM is reanalyzed and a modification is proposed.

The paper is arranged in the following manner. In Sec. II, we present the details of the calculations. Sections III A and III B deal with the linear and second-order optical response of monolayer SL's, respectively. Section IV provides a summary of our work. Appendix A lists all the formulas used for the calculation of the SHG susceptibility. Details of the modifications to the EMM are presented in Appendix B.

II. METHODOLOGY

Total-energy calculations are performed using the FPLAPW method implemented in the WIEN2k code.[57] Thereby the scalar relativistic Kohn-Sham equations are solved in a self-consistent scheme. For the exchange-correlation potential we use the generalized gradient approximation (GGA) derived by Perdew and Wang.[58]

The detailed formalism for the determination of the linear dielectric tensor $\epsilon(\omega)=\epsilon_1(\omega)+i\epsilon_2(\omega)$ within the FPLAPW formalism has been presented before.[59] The susceptibility for the second-harmonic generation $\chi^{(2)}(2\omega,\omega,\omega)$ has been calculated using the an extension to this program.[60] The formulas for calculating $\chi^{(2)}(2\omega,\omega,\omega)$ have also been presented before.[61–64] They are rewritten to improve the computational efficiency, and we compare the computing time for both sets of formulas in Appendix A. The SHG susceptibility obtained satisfies all the theoretical sum rules presented by Scandolo and Bassani.[65]

All the calculations are converged in terms of basis functions as well as in the size of the *k*-point mesh representing the Brillouin zone. The linear optical properties are calculated on a mesh of 500 *k* points in the irreducible Brillouin zone (IBZ), and for the second-order susceptibility a mesh of 1500 *k* points in the IBZ is used.

In all the superlattices, GaP is grown on top of other group III phosphates (InP and AlP) or GaAs as the substrate material. The superstructures are constructed in the (110) direction, which is equivalent to (100) direction in these materials. All these structures are treated in tetragonal unit cells. The details of this unit cell for such SL's have been discussed before [Fig. 1(a) in Ref. 66]. The lattice constants of the SL are estimated using the macroscopic elasticity theory,[34,42,67] and are presented in Table I. The experimental lattice constants of the constituent materials (InP, GaP, AlP, and GaAs) are taken from Ref. 68.

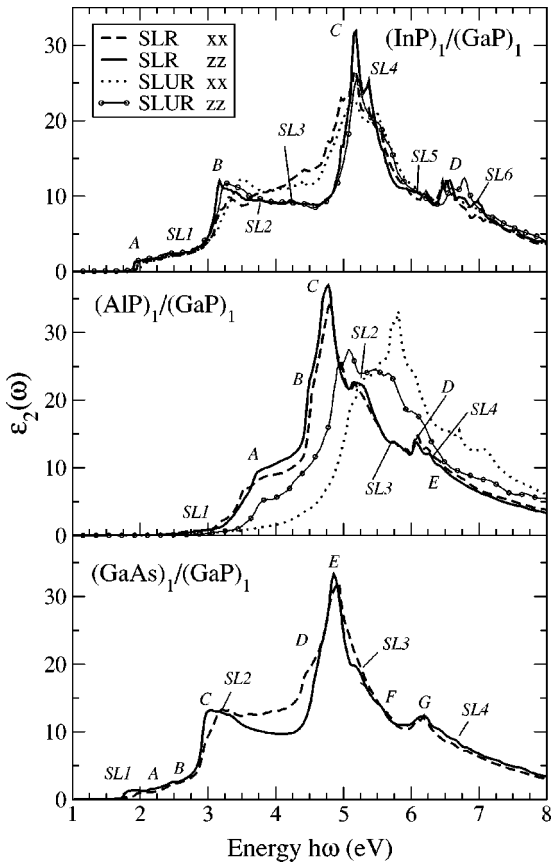

FIG. 1. Components of the imaginary part of the dielectric tensor for the relaxed (SLR) and unrelaxed (SLUR) superlattices for (a) $(InP)_1/(GaP)_1$, (b) $(AlP)_1/(GaP)_1$, and (c) $(GaAs)_1/(GaP)_1$. The important features in $\epsilon_2^{zz}(\omega)$ for the relaxed SL's are labeled with the uppercase letters.

III. RESULTS AND DISCUSSION

A. Linear optical response

First, we shall discuss the importance of lattice relaxations and their effect on the linear optical properties. Total energy and force calculations performed for the unrelaxed atomic positions of the monolayer InP/GaP and AlP/GaP SL's show considerable forces on the atoms, so the relaxation of the structure is needed. On complete relaxation, there is a gain in energy of 0.195 and 1.124 eV per formula unit for $(InP)_1/(GaP)_1$ and $(AlP)_1/(GaP)_1$, respectively. For the case of $(GaAs)_1/(GaP)_1$ the atomic relaxations were not needed.

The imaginary part of the dielectric function $\epsilon_2(\omega)$ for all the SL's under investigation are presented in Fig. 1. All the optical results presented in this paper are scissors corrected[61] using the scissors operator calculated by taking the difference between the theoretical and experimental band gaps of the SL. Among the SL's under investigation for the relaxed structures, the anisotropy in $\epsilon_2(\omega)$ is maximum for $(InP)_1/(GaP)_1$ [Fig. 1(a)], where the lattice mismatch be-

tween InP and GaP is 7.38%, while for $(AlP)_1/(GaP)_1$ [Fig. 1(b)] the anisotropy is minimum and so is the lattice mismatch (0.2%). $(GaAs)_1/(GaP)_1$ [Fig. 1(c)] lies in between the two with a lattice mismatch between GaAs and GaP of 3.66%. These trends indicate that most of the anisotropy is due to the strain in the growth material rather than to the lower symmetry of the superlattice. These results are in accordance with similar observations previously made for GaAs/AlAs and Si/Ge SL's.[55,56] On the other hand, the anisotropy in $\epsilon_2(\omega)$ of the unrelaxed SL's shows a maximum for the SL formed from the materials with minimum lattice mismatch (AlP/GaP). Also $\epsilon_2(\omega)$ of the unrelaxed SL's is lower in terms of peak heights compared to the relaxed SL's. Hence, the lattice relaxations are very important in determining the correct anisotropy and peak heights, and thus all the further calculations are performed for the relaxed SL's. Our results for $\epsilon_2(\omega)$ of $(GaAs)_1/(GaP)_1$ are qualitatively in reasonable agreement with previous calculations by Ghahramani and Sipe.[53] However, the magnitude of the response in the present results is nearly two times that obtained previously. This is expected, since in their work Ghahramani and Sipe pointed out that the LCGO method is not able to reproduce the correct magnitude of the optical response and their results could be underestimated by a factor of 2. The other differences in the two theoretical results are as follows:

(1) The present calculations give one sharp peak around 4.75 eV (labeled E), while previous results show a broad multiple peak structure in $\epsilon_2^{zz}(\omega)$ and $\epsilon_2^{xx}(\omega)$ around the same energy.

(2) In the energy region of 3.2–4.6 eV, $\epsilon_2^{xx}(\omega)$ is greater in magnitude than $\epsilon_2^{zz}(\omega)$ in the present work, whereas the previous results show the opposite. These differences can be due to the difference in the method of calculation. Ghahramani and Sipe have used a non-self-consistent LCGO method within the LDA, while, the present calculations are fully self-consistent using the FPLAPW method within the GGA.

A macroscopic model for the dielectric function of SL's has been suggested by Ghahramani and Sipe.[55] In this model, the SL is considered to be constructed of slabs of an unstrained bulk substrate material (InP, GaAs or AlP in the present case) and a strained bulk material (GaP in the present case) grown on top of the substrate. This model is called the effective medium model (EMM). We have used this model to estimate the macroscopic averaged response and the results are presented in Fig. 2. Like Ghahramani and Sipe[53] we find that the EMM generates reasonably good intensities but poor peak positions in $(GaAs)_1/(GaP)_1$ [Fig. 2(a)]. In the optical spectrum of $(InP)_1/(GaP)_1$ [Fig. 2(b)] and $(AlP)_1/(GaP)_1$ [Fig. 2(c)], the peak positions are better but the intensities are less well described. Another point that should be noted is that for $(AlP)_1/(GaP)_1$, where the lattice relaxations are important, the EMM calculated response is closer to that of the unrelaxed SL than to the relaxed SL response, but the same is not true for $(InP)_1/(GaP)_1$ such that no consistent picture emerges.

In order to find the reason for this behavior, $\epsilon_2^{zz}(\omega)$ for bulk InP, GaAs, and AlP and strained GaP are also presented

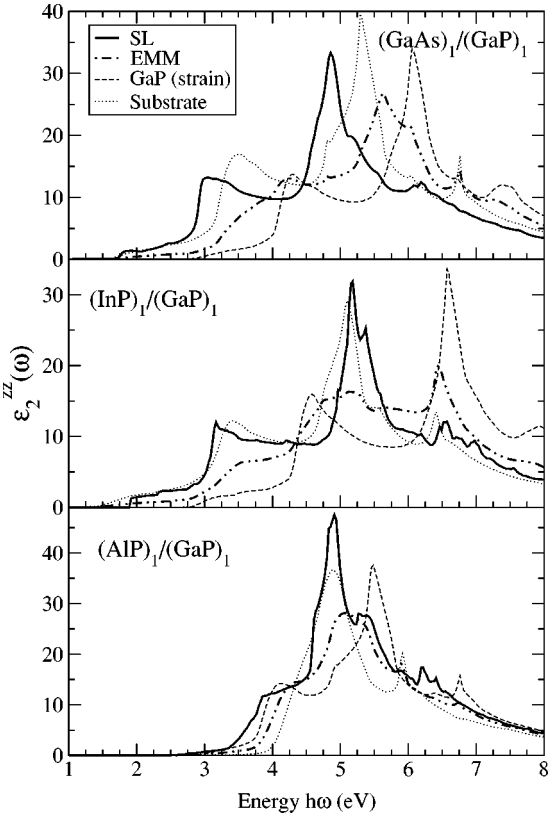

FIG. 2. Frequency dependent $\epsilon_2^{zz}(\omega)$ obtained by the SL calculations compared to the EMM results for (a) $(GaAs)_1/(GaP)_1$, (b) $(InP)_1/(GaP)_1$, and (c) $(AlP)_1/(GaP)_1$. In addition, the data for the bulk GaAs (a), InP(b), AlP(c), and the strained bulk GaP [(a), (b), and (c)] are also presented.

in Fig. 2. We find that if the major peak positions in the dielectric function of the constituent materials are well separated in energy, the EMM gives two separate peaks. As can be seen for the $(InP)_1/(GaP)_1$ the major peaks in the optical spectra of InP and strained GaP are around 5.0 and 6.65 eV, respectively. The EMM also gives two peaks of almost equal strength around 5.0 and 6.65 eV. The separation between the major optical peaks of GaAs and strained GaP is 0.76 eV, and between AlP and strained GaP it is 0.80 eV. The EMM in these cases results in broadened and thus weakened peaks. It is surprising that the SL response is seemingly dominated by the substrate material with the growth material having little $[(GaAs)_1/(GaP)_1]$ to nearly no contribution $[(InP)_1/(GaP)_1]$ (Fig. 2).

The purpose of the model is to find the bulklike features in order to facilitate the detection of true SL features by comparing the model results with the full SL calculations. But EMM takes into account the effect of junction formation only partially by using the strained lattice parameters for one of the constituent materials. This is useful for reproducing the anisotropy. The effect of the junction formation on the band gap, however, is ignored which is taken to be the experimental gap of the unstrained bulk. As the number of SL layers increases this effect diminishes, but in the case of monolayer SL's it is pronounced. So the failure of the model in certain cases is not a surprise. Nevertheless, in order to

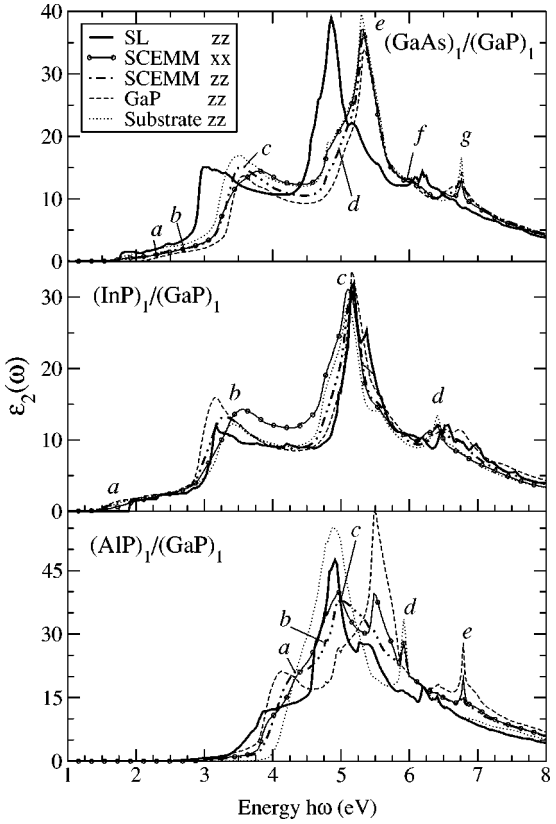

FIG. 3. $\epsilon_2^{zz}(\omega)$ calculated using the full SL and the SCEMM and $\epsilon_2^{xx}(\omega)$ calculated using the SCEMM for (a) $(GaAs)_1/(GaP)_1$, (b) $(InP)_1/(GaP)_1$, and (c) $(AlP)_1/(GaP)_1$. In addition, the data for the bulk GaAs (a), InP(b), AlP(c), and the strained bulk GaP [(a), (b), and (c)] are also presented. The important features in $\epsilon_2^{zz}(\omega)$ for the relaxed SL's obtained by the SCEMM are labeled with the lowercase letters.

provide a simple model for predicting the bulklike features in the SL optical properties on the basis of its constituent materials, the shortcomings of the EMM can be fixed in the following way: The calculations are performed first for the unstrained growth material (GaP in the present case) and the scissors operator is determined by the comparison with the experimental data. Now assuming that GGA (or LDA) underestimates the gap consistently in the unstrained and strained bulk materials, this same scissors operator is used to correct the calculated linear (and nonlinear) optical response of the strained growth material (GaP in the present case). The average of this response with the response of the bulk substrate material (AlP, InP, or GaAs in the present case) is then taken to determine the effective optical response of the SL. We call this new model the strain-corrected effective medium model (SCEMM). The details of the SCEMM are presented in Appendix B. The results of the SCEMM along with the dielectric function of the substrate and strained growth material, corrected by the scissors operator calculated as stated above, are presented in Fig. 3. As can be seen, the model reproduces most of the features in the SL spectra of all the compounds under investigation. The remaining discrepancy in peak positions is due to the fact that the experimental SL gap is lower than the average gap of the constituent materials. More importantly, the SCEMM shows that the SL response is not just dominated by the substrate material, as indicated by the EMM, but has features from both constituent materials. This fact is best seen in the case of $(AlP)_1/(GaP)_1$ where the SCEMM peak labeled with *a* in Fig. 3(c) is dominated by the strained bulk GaP transitions and *c* is bulk InP like. The anisotropy in $\epsilon_2(\omega)$ determined by the SCEMM confirms our earlier observation that most of the anisotropy is due to strain in the growth material rather than due to the lower symmetry of the superlattice. The features not reproduced by the model are referred to as the SL features in the present work. The following features can be identified as SL effects: SL1($\sim$2.5 eV), SL2($\sim$3.75 eV), SL3($\sim$4.25 eV), SL4($\sim$5.6 eV), SL5($\sim$6 eV), and SL6 ($\sim$7 eV) in $(InP)_1/(GaP)_1$, SL1($\sim$2.85 eV), SL2 ($\sim$5.25 eV), SL3($\sim$5.8 eV), and SL4($\sim$6.5 eV) in $(AlP)_1/(GaP)_1$, and SL1($\sim$1.88 eV), SL2($\sim$3.25 eV), SL3($\sim$5.25 eV), and SL4($\sim$6.57 eV) in $(GaAs)_1/(GaP)_1$ SL's in Fig. 1

The real part of the dielectric function in the static limit is a directly measurable quantity. Our calculated results of $\epsilon_1^{xx}(0)$ and $\epsilon_1^{zz}(0)$ for the relaxed SL's are presented in Table II. Two things should be noted. First, the anisotropy in $\epsilon_1(0)$ follows the trend of the lattice mismatch with a maximum of 2.96% for $(InP)_1/(GaP)_1$ and a minimum of 2.60% for $(AlP)_1/(GaP)_1$, while $(GaAs)_1/(GaP)_1$ lies in between the two with an anisotropy in $\epsilon_1(0)$ of 2.80%. Second, in case of $(AlP)_1/(GaP)_1$ and $(GaAs)_1/(GaP)_1$, the lattice constant for the substrate material (GaAs and AlP) is larger than that of the growth material (GaP) and so $\epsilon_1^{xx}(0)$ is greater than $\epsilon_1^{zz}(0)$, while it is just the opposite for AlP/GaP SL. The results of $\epsilon_1(0)$ using the SCEMM are closer to the full SL calculations (worst by a maximum of 6.8%) than the results obtained using the EMM (worst by a maximum of 12.3%). A more important test for any model, however, comes in the determination of the nonlinear optical properties as they are

TABLE II. Static dielectric constants $\epsilon_1^{xx}(0)$ and $\epsilon_1^{zz}(0)$ and the components of the SHG susceptibility in the static limit $\chi_1^{zyx}(0)$ and $\chi_1^{xyz}(0)$ in units of 10^{-8} esu for the relaxed SL's compared to the SCEMM and the EMM results.

Superlattice	$\epsilon_1^{xx}(0)$			$\epsilon_1^{zz}(0)$			$\chi_1^{zyx}(0)$			$\chi_1^{xyz}(0)$		
	SL	SCEMM	EMM	SL	SCEMM	EMM	SL	SCEMM	EMM	SL	SCEMM	EMM
InP/GaP	9.27	9.60	8.51	9.00	9.30	8.17	13.89	15.57	9.47	10.42	15.55	9.29
AlP/GaP	8.65	8.25	8.27	8.86	8.28	8.30	6.34	6.08	6.14	7.51	6.10	6.16
GaAs/GaP	10.48	9.76	9.23	10.19	9.54	8.93	16.65	11.4	9.14	15.56	11.40	8.95

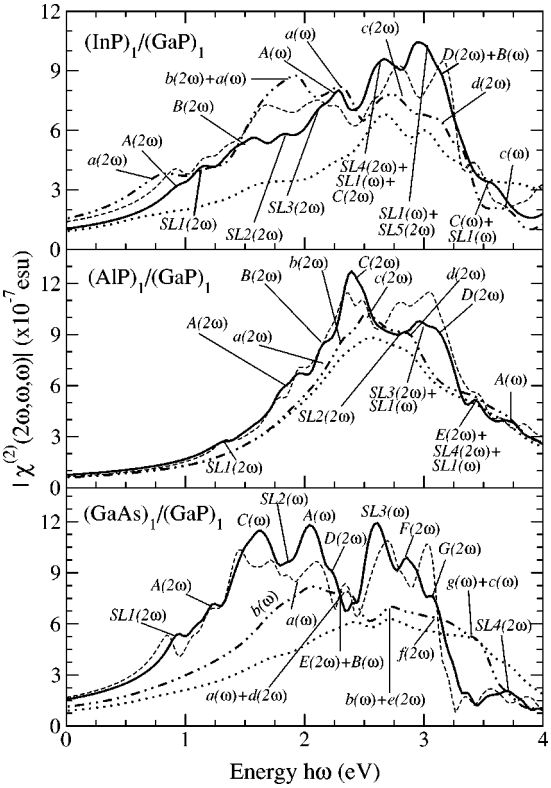

FIG. 4. (a) The two inequivalent components of susceptibility for the SHG $|\chi^{(2)}_{xyz}(2\omega,\omega,\omega)|$ (thick solid line) and $|\chi^{(2)}_{zyx}(2\omega,\omega,\omega)|$ (dashed line) obtained from the full SL calculations, along with the SCEMM (thick dash-dot line) and the EMM (dotted line) results of $|\chi^{(2)}_{xyz}(2\omega,\omega,\omega)|$ for $(\mathrm{InP})_1/(\mathrm{GaP})_1$. (b) The same for $(\mathrm{AlP})_1/(\mathrm{GaP})_1$. (c) The same for $(\mathrm{GaAs})_1/(\mathrm{GaP})_1$.

much more sensitive to the small changes in the bandstructure than the linear optical spectra.

B. Second-order optical response

The magnitude of the SHG susceptibility $\chi^{(2)}(2\omega,\omega,\omega)$ for the monolayer SL's along with the results of the SCEMM and the EMM are presented in Fig. 4. The peaks in $\chi^{(2)}(2\omega,\omega,\omega)$ can be identified to be coming from 2ω and/or ω resonances of the peaks in the linear dielectric function. Therefore, this identification of the peaks in the SHG susceptibility is done from the respective linear optical spectra. The identified peaks are marked in Fig. 4 and the nomenclature adopted is $M(x\omega)+N(y\omega)$, which indicates that the peak comes from an $x\omega$ resonance of the peak M with the $y\omega$ resonance of peak N in the linear optical spectra. For example, for $(\mathrm{InP})_1/(\mathrm{GaP})_1$ [Fig. 4(a)] the hump just below 1 eV, labeled as $A(2\omega)$ in the $\chi^{(2)}_{xyz}(2\omega,\omega,\omega)$ component for the SL comes from the 2ω resonance of the peak labeled as A in the linear optical spectra [Fig. 1(a)]. The peak at 1.15 eV is an SL peak, labeled as $\mathrm{SL1}(2\omega)$, coming from the 2ω resonance of the peak labeled as SL1 in the $\epsilon_2(\omega)$ plot [Fig. 1(a)]. Similarly, all other features have been identified and marked in Fig. 4(a). As expected, the pure SL peaks $\mathrm{SL1}(2\omega)$, $\mathrm{SL2}(2\omega)$, $\mathrm{SL3}(2\omega)$, and $\mathrm{SL1}(\omega)+\mathrm{SL5}(2\omega)$ are absent in the SCEMM results. The features coming from resonances of the SL and bulklike peaks such as $\mathrm{SL4}(2\omega)+\mathrm{SL1}(\omega)+C(2\omega)$ and $C(\omega)+\mathrm{SL1}(2\omega)$ are underestimated by the SCEMM as features of $c(2\omega)$ and $c(\omega)$, while the peaks coming from the 2ω and/or ω resonances of the bulk peaks are well reproduced by the SCEMM. The peak labeled as $a(2\omega)$ is more pronounced than the corresponding SL peak $A(2\omega)$ in accordance with a [Fig. 3(b)] being larger than A [Fig. 1(a)] in the linear optical spectra. In contrast, the peak labeled as $B(2\omega)$ is smaller than the corresponding SCEMM peak $b(2\omega)+a(\omega)$, since the SCEMM peak is due to the ω resonance of peak a with the 2ω resonance of the peak labeled as b in the linear dielectric function [Fig. 3(b)]. A similar feature assignment for the $(\mathrm{AlP})_1/(\mathrm{GaP})_1$ and $(\mathrm{GaAs})_1/(\mathrm{GaP})_1$ monolayer SL's is also performed and the details are marked in Figs. 4(b) and 4(c). The same trends are observed in all the materials under investigation, with the SCEMM reproducing all the peaks other than the pure SL features. This indicates that the SCEMM can be used to identify the structure in the optical spectra coming from the bulklike transitions and hence facilitating the determination of the SL effects like symmetry lowering. The EMM on the other hand is not able to reproduce all the non-SL features, and is therefore not a good model for the monolayer SL's.

Our results for the magnitude of $\chi^{(2)}(2\omega,\omega,\omega)$ of $(\mathrm{GaAs})_1/(\mathrm{GaP})_1$ [Fig. 4(c)] differ from previous calculations are given below.[53]

(1) $\chi^{(2)}{}_{xyz}(2\omega,\omega,\omega)$ is generally in good agreement with the previous work in terms of peak heights as well as positions. The only difference is the appearance of two extra features in the present work, i.e., a hump at $\sim$1.25 eV $[A(2\omega)]$ and a peak at 1.75 eV $[\mathrm{SL1}(\omega)]$.

(2) In the present work the anisotropy in the nonlinear optical response is found to be more pronounced compared to the work of Ghahramani and Sipe. As it is well known, the nonlinear optical properties are more sensitive to the small changes in the bandstructure than the linear ones so any anisotropy in the linear optical response is expected to be enhanced in the nonlinear spectra. This is in accordance with our findings, while the previous work shows the opposite.

(3) Our results for $\chi^{(2)}{}_{zyx}(2\omega,\omega,\omega)$ differ substantially from the previous results, but since a detailed identification of the peaks is not presented previously, it is difficult to point out the discrepancies. As mentioned earlier, these differences could be due to the different methods used.

Finally, the SHG susceptibility in the static limit is presented in Table II. The maximum anisotropy in $\chi^{(2)}(0)$ is in $(\mathrm{InP})_1/(\mathrm{GaP})_1$ (28.5%) and the minimum is found for $(\mathrm{GaAs})_1/(\mathrm{GaP})_1$ (12.8%). $(\mathrm{AlP})_1/(\mathrm{GaP})_1$ has an anisotropy of 16.8%. Neither EMM nor SCEMM give results close to the SL results. This is in contradiction with the previous findings,[53] where Ghahramani and Sipe report the EMM to give (Table III) results within 5% of the SL data. The failure of the SCEMM and the EMM in the present case is not surprising, since both the models fail to reproduce some of the main features in the optical spectra leading to a substantial difference in the static limit. But still the SCEMM results are an improvement over the EMM.

TABLE III. Number of k points in the IBZ, number of valence bands (VB), number of conduction bands (CB), CPU time (in minutes) needed to calculate the SHG susceptibility using Eqs. (A1)–(A3) and Eqs. (A9)–(A11).

k points	Number of bands		CPU	Time
IBZ	VB	CB	Eqs. (A1)–(A3)	Eqs. (A9)–(A11)
385	9	11	11.02	2.67
385	9	5	4.50	1.10
146	9	11	3.50	0.88
146	24	33	88.01	19.47

IV. SUMMARY

To summarize, we have performed calculations for the linear and nonlinear optical properties of some III-V monolayer SL's. We conclude the following.

(1) The lattice relaxations play an important role in the determination of the correct anisotropy and peak heights of the linear optical spectra.

(2) The effective medium model (EMM) does not reproduce the correct bulk features mainly because it assumes that the optical band gap of the material does not change with strain, and is taken as the experimental direct gap of the unstrained material.

(3) An improvement over this model is the strain-corrected effective-medium model (SCEMM), which correctly averages the optical properties of the constituent materials of the SL and facilitates the identification of the SL features in the optical spectra.

(4) The SCEMM results confirm that most of the anisotropy in $\epsilon(\omega)$, in the SL's under investigation, comes from the strain in the growth material rather than the symmetry lowering due to SL formation.

(5) The anisotropy in $\epsilon_2(\omega)$ and, in particular, in $\epsilon_2(0)$ follow the trend in the lattice mismatch being maximum for $(\mathrm{InP})_1/(\mathrm{GaP})_1$ and minimum for $(\mathrm{AlP})_1/(\mathrm{GaP})_1$.

(6) The small SL features in $\epsilon_2(\omega)$ are greatly enhanced in the nonlinear spectra and the same is true for the anisotropy.

(7) The SCEMM is able to correctly reproduce all the bulklike features in the SHG susceptibility, whereas pure SL features are absent and features coming from the resonance of the SL and bulklike transitions are underestimated. This leads to a failure of the SCEMM (as well as EMM) in the determination of $\chi^{(2)}(0)$. But the SCEMM is still an improvement over the EMM.

(8) The SCEMM is good for determining the linear optical properties of the SL's, but for the correct determination of the nonlinear optical properties SL calculations are essential. The effects of strain due to junction formation and the lattice relaxations are expected to decrease with increase in the layer thickness. It would be interesting to compare two models in such a case and to find the SL period, for which these effects become insignificant.

(9) Although no experimental measurements of the SHG susceptibilty for the compounds under investigation exist, a detailed comparison of future experimental data with theoretical results would help in the identification of various features in the optical spectra, in particular, to highlight the effect of the interface formation in the SL's. This would lead to a better understanding of the physical properties, which is one of the most essential ingredient for tailorable materials of technological importance.

ACKNOWLEDGMENTS

We would like to thank the Austrian Science Fund (Project No. P13430) for financial support. The code for calculating nonlinear optical properties was written under the EXCITING network funded by the EU (Contract No. HPRN-CT-2002-00317). S.S. would also like to thank Bernd Olejnik for useful discussions and suggestions during the course of code development.

APPENDIX A: FORMALISM FOR THE SECOND-ORDER RESPONSE

The formulas for the total susceptibility for the second-harmonic generation (SHG) for clean semiconductors have been presented before.[61,62] We note that Eq. (B3) of Ref. 61 is incorrect, and the correct form of this equation can be obtained from the sum of Eqs. (B16b) and (B17) of Ref. 62. The susceptibility for the SHG can be divided into three major contributions: the interband transitions $\chi_{\mathrm{inter}}(2\omega,\omega,\omega)$, the intraband transitions $\chi_{\mathrm{intra}}(2\omega,\omega,\omega)$, and the modulation of interband terms by intraband terms $\chi_{\mathrm{mod}}(2\omega,\omega,\omega)$,

$$\chi^{abc}_{\mathrm{inter}}(2\omega,\omega,\omega)=\frac{e^3}{\hbar^2}\sum_{nml}{}'\int\frac{d\mathbf{k}}{4\pi^3}\frac{r^a_{nm}\{r^b_{ml}r^c_{ln}\}}{(\omega_{ln}-\omega_{ml})}\left\{\frac{2f_{nm}}{(\omega_{mn}-2\omega)}+\frac{f_{ml}}{(\omega_{ml}-\omega)}+\frac{f_{ln}}{(\omega_{ln}-\omega)}\right\}, \tag{A1}$$

$$\chi^{abc}_{\mathrm{intra}}(2\omega,\omega,\omega)=\frac{e^3}{\hbar^2}\int\frac{d\mathbf{k}}{4\pi^3}\left[\sum_{nml}{}'\omega_{mn}r^a_{nm}\{r^b_{ml}r^c_{ln}\}\left\{\frac{f_{nl}}{\omega^2_{ln}(\omega_{ln}-\omega)}-\frac{f_{lm}}{\omega^2_{ml}(\omega_{ml}-\omega)}\right\}-8i\sum_{nm}{}'\frac{f_{nm}r^a_{nm}\{\Delta^b_{mn}r^c_{mn}\}}{\omega^2_{mn}(\omega_{mn}-2\omega)}\right.$$
$$\left.+2\sum_{nml}{}'\frac{f_{nm}r^a_{nm}\{r^b_{ml}r^c_{ln}\}(\omega_{ml}-\omega_{ln})}{\omega^2_{mn}(\omega_{mn}-2\omega)}\right], \tag{A2}$$

$$\chi^{abc}_{\rm mod}(2\omega,\omega,\omega)=\frac{e^3}{2\hbar^2}\int\frac{d\mathbf{k}}{4\pi^3}\left[\sum_{nml}{}'\frac{f_{nm}}{\omega^2_{mn}(\omega_{mn}-\omega)}\{\omega_{nl}r^a_{lm}\{r^b_{mn}r^c_{nl}\}-\omega_{lm}r^a_{nl}\{r^b_{lm}r^c_{mn}\}\}-i\sum_{nm}{}'\frac{f_{nm}r^a_{nm}\{r^b_{mn}\Delta^c_{mn}\}}{\omega^2_{mn}(\omega_{mn}-\omega)}\right] \tag{A3}$$

for all $n\neq m\neq l$. The symbols are defined as

$$\Delta^a_{nm}(\mathbf{k})=v^a_{nn}(\mathbf{k})-v^a_{mm}(\mathbf{k}) \tag{A4}$$

with v^a_{nm} being the a component of the electron velocity given as

$$v^a_{nm}(\mathbf{k})=iw_{nm}(\mathbf{k})r^a_{nm}(\mathbf{k}) \tag{A5}$$

and

$$\{r^a_{nm}(\mathbf{k})r^b_{ml}(\mathbf{k})\}=\frac{1}{2}[r^a_{nm}(\mathbf{k})r^b_{ml}(\mathbf{k})+r^b_{nm}(\mathbf{k})r^a_{ml}(\mathbf{k})]. \tag{A6}$$

The position matrix elements between states n and m, $r^a_{nm}(\mathbf{k})$, are calculated from the momentum matrix element p^a_{nm} using the relation[59]

$$r^a_{nm}(\mathbf{k})=\frac{p^a_{nm}(\mathbf{k})}{im\omega_{nm}(\mathbf{k})} \tag{A7}$$

for all $\omega_n(\mathbf{k})\neq\omega_m(\mathbf{k})$ and $r^a_{nm}(\mathbf{k})=0$, otherwise with the energy difference between the states n and m given by

$$\hbar\omega_{nm}=\hbar(\omega_n-\omega_m). \tag{A8}$$

For the sake of clarity, the $\mathbf{k}$ dependence of ω_{nm}, p^a_{nm}, v^a_{nm}, and Δ_{nm} in Eqs. (A1)–(A3) are suppressed. Equations (A1)–(A3) are computationally very demanding since n, l, and m run over all the bands. But this requirement can be relaxed by adjusting the equations slightly using the fact that the equations are symmetric in n, l, and m, and hence the indices can be interchanged. At the same time one can get rid of the Fermi functions. Equations (A1)–(A3) then read

$$\chi^{abc}_{\rm inter}(2\omega,\omega,\omega)=\frac{e^3}{\hbar^2\Omega}\sum_{nml}{}'\sum_{\mathbf{k}}W_{\mathbf{k}}\left\{\frac{2r^a_{nm}\{r^b_{ml}r^c_{ln}\}}{(\omega_{ln}-\omega_{ml})(\omega_{mn}-2\omega)}-\frac{1}{(\omega_{mn}-\omega)}\left[\frac{r^c_{lm}\{r^a_{mn}r^b_{nl}\}}{(\omega_{nl}-\omega_{mn})}-\frac{r^b_{nl}\{r^c_{lm}r^a_{mn}\}}{(\omega_{lm}-\omega_{mn})}\right]\right\}, \tag{A9}$$

$$\chi^{abc}_{\rm intra}(2\omega,\omega,\omega)=\frac{e^3}{\hbar^2\Omega}\sum_{\mathbf{k}}W_{\mathbf{k}}\left\{\sum_{nml}{}'\frac{1}{\omega^2_{mn}(\omega_{mn}-\omega)}[\omega_{ln}r^b_{nl}\{r^c_{lm}r^a_{mn}\}-\omega_{ml}r^c_{lm}\{r^a_{mn}r^b_{nl}\}]-8i\sum_{nm}{}'\frac{1}{\omega^2_{mn}(\omega_{mn}-2\omega)}r^a_{nm}\{r^b_{ml}r^c_{ln}\}\right.$$
$$\left.+2\sum_{nml}{}'\frac{r^a_{nm}\{r^b_{ml}r^c_{ln}\}(\omega_{ml}-\omega_{ln})}{\omega^2_{mn}(\omega_{mn}-2\omega)}\right\}, \tag{A10}$$

$$\chi^{abc}_{\rm mod}(2\omega,\omega,\omega)=\frac{e^3}{2\hbar^2\Omega}\sum_{\mathbf{k}}W_{\mathbf{k}}\left\{\sum_{nml}\frac{1}{\omega^2_{mn}(\omega_{mn}-\omega)}[\omega_{nl}r^a_{lm}\{r^b_{mn}r^c_{nl}\}-\omega_{lm}r^a_{nl}\{r^b_{lm}r^c_{mn}\}]-i\sum_{nm}\frac{r^a_{nm}\{r^b_{mn}\Delta^c_{mn}\}}{\omega^2_{mn}(\omega_{mn}-\omega)}\right\}, \tag{A11}$$

where Ω is the unit cell volume, $W_{\mathbf{k}}$ is the weight of k point and n denotes the valence states, m denotes the conduction states, and l denotes all states ($l\neq m,n$). We have used Eqs. (A9)–(A11) to calculate the total susceptibility. We also confirm that the real and imaginary parts of this susceptibility satisfy all the sum rules presented by Scandolo and Bassani.[65] Some results of the benchmark are presented in the following table. All the calculations are performed with a mesh of 1000 points in the energy interval 0.0–4.0 eV on an SGI R12000 processor.

APPENDIX B: FORMALISM FOR THE STRAIN-CORRECTED EFFECTIVE-MEDIUM MODEL

The expression for calculating the xx component of the linear optical response using the effective medium model is[55]

$$\epsilon^{eff}_T(\omega,\delta,\Delta)=\frac{1}{2}[\epsilon^{xx}_A(\omega,\delta)+\epsilon^{xx}_B(\omega,\Delta)], \tag{B1}$$

which can be obtained from the continuity of the tangential electric field across the interface $E_T=E^A_T$ and $E_T=E^B_T$ and the expression for the average-induced polarization $P^{eff}=\frac{1}{2}(P^A+P^B)$. The longitudinal electric field on the other hand is given by $\epsilon^{zz}_{eff}E_L=\epsilon^{zz}_AE^A_L=\epsilon^{zz}_BE^B_L$, and so the expression for ϵ^{eff}_{zz} is given by

$$\epsilon^{eff}_{zz}(\omega,\delta,\Delta)=\frac{2\epsilon^{xx}_A(\omega,\delta)\epsilon^{xx}_B(\omega,\Delta)}{\epsilon^{xx}_A(\omega,\delta)+\epsilon^{xx}_B(\omega,\Delta)}. \tag{B2}$$

Here it is assumed that A is the substrate material and B is the material grown on top of A, and hence has the strained lattice parameters. $\epsilon^{xx}_A(\omega,\delta)$ is the xx component of the frequency-dependent dielectric tensor for material A (or

strained material B) corrected with the scissors operator δ (or Δ). Where δ and Δ are calculated as

$$\delta = XDG - TOG_X, \tag{B3}$$

$$\Delta = XDG - TOG_S, \tag{B4}$$

where XDG is the experimental direct band gap and TOG is the optical bang gap calculated theoretically. The subscripts X and S indicate that the experimental lattice parameters and the strained lattice parameters, respectively, are used for calculating the theoretical optical band gap. The EMM assumes that even after straining, the material B has the same gap as measured experimentally for the unstrained material. These expressions are slightly altered for the SCEMM reading,

$$\epsilon_T^{eff}(\omega,\delta) = \frac{1}{2}[\epsilon_A^{xx}(\omega,\delta_A) + \epsilon_B^{xx}(\omega,\delta_B)], \tag{B5}$$

$$\epsilon_{zz}^{eff}(\omega,\delta) = \frac{2\epsilon_A^{xx}(\omega,\delta_A)\epsilon_B^{xx}(\omega,\delta_B)}{\epsilon_A^{xx}(\omega,\delta_A) + \epsilon_B^{xx}(\omega,\delta_B)}, \tag{B6}$$

where the symbols have the usual meaning. One extra set of calculations is needed for the unstrained B material to determine the optical band gap and hence the scissors operator. Then the calculations are performed for the strained material B and the band gap is corrected with the ''old'' scissors operator. This effective zz component of the dielectric tensor can be used to calculate the xyz component of the SHG susceptibility as follows:

$$\chi_{xyz}^{eff}(2\omega,\omega,\omega,\delta) = \frac{\epsilon_{zz}^{eff}(\omega,\delta)}{2}\left[\frac{\chi_{xyz}^{A}(2\omega,\omega,\omega,\delta_A)}{\epsilon_{zz}^{A}(\omega,\delta_A)} + \frac{\chi_{xyz}^{B}(2\omega,\omega,\omega,\delta_B)}{\epsilon_{zz}^{B}(\omega,\delta_B)}\right]. \tag{B7}$$

*Electronic address: sangeeta.sharma@uni-graz.at

[1] G.C. Osbourn, J. Vac. Sci. Technol., B **1**, 379 (1983).

[2] *Molecular Beam Epitaxy and Heterostructures*, edited by L.L. Chang and K. Ploog (Nijhoff, Dordrecht, 1985).

[3] T.P. Pearsall, J. Bevk, L.C. Feldman, J.M. Bonar, J.P. Mannaerts, and A. Ourmazd, Phys. Rev. Lett. **58**, 729 (1987).

[4] *Interfaces, Quantum Wells, and Superlattices*, edited by C.R. Leavens and R. Taylor (Plenum, New York, 1988).

[5] *Band Structure Engineering in Semiconductor Microstructures*, edited by R.A. Abram and M. Jaros (Plenum, New York, 1989).

[6] A. Mascarenhas, R.G. Alonso, G.S. Horner, S. Froyen, K.C. Hsieh, and K.Y. Cheng, Phys. Rev. B **48**, 4907 (1993).

[7] *Heterojunctions Band Discontinuities. Physics and Devices Applications*, edited by F. Capasso and G. Margaritonodo (North-Holland, Amsterdam, 1987).

[8] C. Angus and C.C. Hayman, Science (Washington, DC, U.S.) **241**, 877 (1988).

[9] K. Uchida, N. Miura, T. Sugita, F. Issiki, N. Usami, and Y. Shiraki, Physica B **249**, 909 (1998).

[10] F. Issiki, S. Fukatsu, T. Ohta, and Y. Shiraki, Solid-State Electron. **40**, 43 (1996).

[11] Y. Nabetani, A. Wakahara, and A. Sasaki, Mater. Sci. Eng., B **35**, 454 (1995).

[12] E.G. Wang and C.S. Ting, Appl. Phys. Lett. **66**, 1400 (1995).

[13] X.L. Wang, A. Wakahara, and A. Sasaki, Appl. Phys. Lett. **65**, 2096 (1994).

[14] A. Morii, T. Takano, J. Kitamura, K. Hara, H. Kukimoto, J. Yoshino, and T. Yasuda, Solid-State Electron. **37**, 649 (1994).

[15] E.G. Wang, Li.Y. Zhang, and H.Y. Wang, Chin. Phys. **11**, 586 (1991).

[16] A. Gomyo, T. Suzuki, and S. Iijima, Phys. Rev. Lett. **60**, 2645 (1988).

[17] H.M. Cheong, Y. Zhang, A.G. Norman, J.D. Perkins, A. Mascarenhas, K.Y. Cheng, and K.C. Hsieh, Phys. Rev. B **60**, 4883 (1999).

[18] D.H. Rich, Y. Tang, and H.T. Lin, J. Appl. Phys. **81**, 6837 (1997).

[19] Y. Tang, D.H. Rich, A.M. Moy, and K.Y. Cheng, J. Vac. Sci. Technol., B **15**, 1034 (1997).

[20] Y. Tang, H.D. Lin, D.H. Rich, P. Colter, and S.M. Vernon, Phys. Rev. B **53**, 10 501 (1996).

[21] M. Fudeta, H. Asahi, S.J. Kim, J.H. Noh, K. Asami, and S.I. Gonda, Jpn. J. Appl. Phys., Part 1 **38**, 1078 (1999).

[22] S.J. Kim, H. Asahi, K. Asami, M. Takemoto, M. Fudeta, and S. Gonda, Appl. Surf. Sci. **130**, 729 (1998).

[23] S.J. Kim, H. Asahi, K. Asami, M. Takemoto, M. Fudeta, and S. Gonda, Jpn. J. Appl. Phys., Part 1 **37**, 1540 (1998).

[24] H.P. Zhou and T.C.M. Sotomayor, Proc. SPIE **1675**, 186 (1992).

[25] M. Recio, G. Armelles, J. Melendez, and F. Briones, J. Appl. Phys. **67**, 2044 (1990).

[26] A. Chavez-Prison, J. Yumoto, H. Ando, T. Fukui, and H. Kanbe in *Science and Tecnology of Mesoscopic Structures*, edited by S. Namba, C. Hamaguchi, and T. Ando (Springer-Verlag, 1992).

[27] Y.C.A. Shih, K. Sadra, and B.G. Streetman, J. Vac. Sci. Technol. B **12**, 1082 (1994).

[28] N.V. Nguyen, J.G. Pellegrino, P.M. Amritraj, D.G. Seiler, and S.B. Qadri, J. Appl. Phys. **73**, 7739 (1993).

[29] P.W.M. Blom, C. Smit, J.E.M. Haverkort, and J.H. Wolter, Appl. Phys. Lett. **62**, 2393 (1993).

[30] Yu. Pusep, A. Milekhin, and A. Poropov, Superlattices Microstruct. **13**, 115 (1993).

[31] A. Vercik and Y.G. Galvao, Braz. J. Phys. **32**, 331 (2002).

[32] B.Q. Sun, J.N. Wang, D.S. Jiang, J.Q. Wu, Y.Q. Wang, and W.K. Ge, Physica B **279**, 220 (2000).

[33] A. Franceschetti and A. Zunger, Nature (London) **402**, 60 (1999).

[34] C.G. Van de Walle and R.M. Martin, Phys. Rev. B **34**, 5621 (1986).

[35] C.G. Van de Walle and R.M. Martin, Phys. Rev. B **35**, 8154 (1987).

[36] N. Chetty, A. Munoz, and R.M. Martin, Phys. Rev. B **41**, 2976 (1990).

[37] B.K. Agrawal, S. Agrawal, and R. Srivastava, Surf. Sci. **424**, 232 (1999).

[38] R.G. Dandrea and A. Zunger, Phys. Rev. B **43**, 8962 (1991).

[39] Y. Tanida and M. Ikeda, Phys. Rev. B **50**, 10 958 (1994).

[40] C.H. Park and K.J. Chang, Phys. Rev. B **47**, 12 709 (1993).

[41] T. Kurimoto and N. Hamada, Phys. Rev. B **40**, 3889 (1989).

[42] J. Arriga, M.C. Munoz, V.R. Velasco, and F. Garca-Moliner, Phys. Rev. B **43**, 9626 (1991).

[43] A. Franceschetti and A. Zunger, Appl. Phys. Lett. **65**, 2990 (1994).

[44] Y. Kobayashi, T. Nakayama, and H. Kamimura, J. Phys. Soc. Jpn. **65**, 3599 (1996).
[45] J.H. Yee, G.H. Khanaka, W.T. White, and O.J. Orvis, Phys. Status Solidi B **180**, 135 (1993).
[46] U. Schmid, N.E. Christensen, M. Cardona, F. Luke, and K. Ploog, Phys. Rev. B **45**, 3546 (1992).
[47] M. Kumagai, T. Takagahara, and E. Hanamura, Solid State Commun. **64**, 659 (1987).
[48] M. Kumagai, T. Takagahara, and E. Hanamura, Phys. Rev. B **37**, 898 (1988).
[49] N. Tit, Proc. SPIE **3491**, 767 (1998).
[50] S. Botti and L.C. Andreani, Phys. Rev. B **63**, 235313 (2001).
[51] K. Kawashima and K. Fujiwara, Microelectron. Eng. **43**, 131 (1998).
[52] G. Shibata, T. Nakayama, and H. Kamimura, Jpn. J. Appl. Phys., Part 1 **33**, 6121 (1994).
[53] Ed. Ghahramani and J.E. Sipe, Phys. Rev. B **46**, 1831 (1992).
[54] Ed. Ghahramani, D.J. Moss, and J.E. Sipe, Phys. Rev. B **43**, 8990 (1991).
[55] Ed. Ghahramani, D.J. Moss, and J.E. Sipe, Phys. Rev. B **41**, 5112 (1990).
[56] Ed. Ghahramani, D.J. Moss, and J.E. Sipe, Phys. Rev. B **43**, 9269 (1991).
[57] P. Blaha, K. Schwarz, G.K.H. Madsen, D. Kvasnicka, and J. Luitz, WIEN2k, Vienna University of Technology An Augmented Plane Wave Plus Local Orbitals Program for Calculating Crystal Properties revised edition 2001.
[58] J.P. Perdew and Y. Wang, Phys. Rev. B **45**, 13 244 (1992).
[59] C. Ambrosch-Draxl and J.O. Sofo (unpublished).
[60] S. Sharma (unpublished), see http://www.exciting.physics.at/
[61] J.L.P. Hughes and J.E. Sipe, Phys. Rev. B **53**, 10 751 (1996).
[62] J.E. Sipe and Ed. Ghahramani, Phys. Rev. B **48**, 11 705 (1993).
[63] J.E. Sipe and A.I. Shkrebtii, Phys. Rev. B **61**, 5337 (2000).
[64] S.N. Rashkeev, W.R.L. Lambrecht, and B. Segall, Phys. Rev. B **57**, 3905 (1998).
[65] S. Scandolo and F. Bassani, Phys. Rev. B **51**, 6925 (1995).
[66] S. Ciraci and I.P. Batra, Phys. Rev. B **38**, 1835 (1988).
[67] R. People, Phys. Rev. B **32**, 1405 (1985).
[68] M.Z. Huang and W.Y. Ching, Phys. Rev. B **47**, 9449 (1993), and references therein.